Int. J. Heat Mass Transfer. Vol. 36, No. 2, pp. 423–435, 1993
Printed in Great Britain

0017-9310/93 $6.00 + 0.00

Hydrodynamic stability of multiple steady-states of vertical buoyancy-induced flows in cold pure water

YOUNGKYU HWANG
Department of Mechanical Design, Sung Kyun Kwan University, Suwon 440-746, S. Korea

and

NICHOLAS D. KAZARINOFF† and JOSEPH C. MOLLENDORF‡
†Department of Mathematics and ‡Department of Mechanical and Aerospace Engineering, State University of New York at Buffalo, Amherst, NY 14260, U.S.A.

(*Received* 31 *May* 1991 *and in final form* 3 *February* 1992)

Abstract—Numerical solutions of the hydrodynamic stability equations which model disturbances in steady-state, laminar flows generated by natural convection of cold, pure water adjacent to a vertical, planar, isothermal surface have been obtained. The results yield neutral stability curves representing the relative hydrodynamic stability of the two previously predicted multiple, steady-state base flows. These two steady states are called the upper- and lower-branch solutions (the upper-branch solution has the higher heat transfer rate ($-\theta_b'(0)$) at the vertical isothermal surface). New results presented here include the first hydrodynamic stability analysis for cold water which includes the range of ambient temperature (T_∞) 5.6896–8.0586°C (if the plate temperature T_0 is 0°C), where inside buoyancy force reversals exert a strong influence upon the flow. This range corresponds to values of the density extremum parameter $R = (T_m - T_\infty)/(T_0 - T_\infty)$ in the interval (0.29181, 0.50) where T_m is the density extremum temperature. The results show that for the flows corresponding to the upper- and lower-branch solutions, the critical Grashof number systematically decreases as the heat transfer rate decreases. Namely, an increase in the magnitude of inside buoyancy force reversals, which are associated with the locations of the two points of inflection in the vertical velocity components of the base flow, always cause the flows to be significantly more unstable. The flows corresponding to the upper-branch solutions were, in general, found to be more stable than the flows corresponding to the lower-branch solutions. This agrees with previously reported configurational stability results. The present results also indicate that oscillation between the upper and the lower steady-states is possible (inasmuch as it is consistent with hydrodynamic stability theory) in the range $0.29181 \leqslant R < 0.34$, but not for $R \geqslant 0.34$.

1. INTRODUCTION

NATURAL convection flows in cold water commonly exist around us. The phenomena of instability and transition of these flows are of particular interest, since these flows arise in many applications, both in the environment and in technology [1, 2].

Pure water has a density extremum near 4°C. This behavior dramatically affects the stability characteristics of natural convection flows in cold water. The occurrence of buoyancy force reversals across a thermal boundary layer, leading to reversals in the flows, complicates their stability analysis. The need for classical stability analyses concerning these complex processes is evident. Our study is the first to analyze the neutral stability of laminar, vertical natural convection flows in cold pure water in the presence of buoyancy force reversals. In this first part we treat the case of downflow.

The present study is the instance in which the stability equations have been solved using an adequate computing code (COLSYS) designed to accurately solve two-point boundary-value problems [3], in contrast to previous investigators cited below, who also did numerical studies. Moreover, our results are new in that we have analyzed the neutral stability of both multiple steady-state solutions found in this problem by El-Henawy *et al.* [4].

Most of the past stability studies utilize the Boussinesq formulation of the density as a linear function of temperature, such as for flows in air, warm water etc.; for example, Nachtsheim [5], Hieber and Gebhart [6], Jaluria and Gebhart [7], and Jang [8]. More recently, Gebhart and Mahajan [9] and Gebhart *et al.* [2] have comprehensively reviewed the literature on the stability of natural convection flows in this regard by discussing calculations and observations of amplification of disturbances.

In the present study, the system under consideration (as seen in Fig. 1) is quiescent, cold, pure water adjacent to a vertical, planar, isothermal, impermeable surface. In this situation the Boussinesq approximation does not accurately express the buoyancy force. This is so because if the variation of local temperature T spans the temperature at the density extremum T_m of cold pure water (its density is maximum at

NOMENCLATURE

A	wave number parameter, see equation (19)
A_j	A at G_{xj} $(j = 1, 2, 3)$
B	frequency parameter, see equation (18)
B^*	B at G_{cr}
B_j	B at $G_{\beta j}$ $(j = 1, 2, 3)$
c	wave speed
c_1, c_2, c_3	complex constants
D	characteristic length
$f(\eta)$	generalized stream function
f	physical frequency
g	acceleration due to gravity
G	modified Grashof number, $4(Gr_x/4)^{1/4}$
G_{cr}	critical Grashof number
$Gr(x)$	local Grashof number
(G_{xj}, α_j)	crossing points of the upper- and lower-branch solutions in the (G, α)-neutral stability plane $(j = 1, 2, 3)$
$(G_{\beta j}, \beta_j)$	crossing points of the upper- and lower-branch solutions in the (G, β)-neutral stability plane $(j = 1, 2, 3)$
$H(\eta)$	nondimensional disturbance pressure amplitude function
$\bar{H}(y)$	disturbance pressure amplitude function
i	$\sqrt{(-1)}$
k_1, k_2	constants, see equations (14) and (15)
M	largest magnitude of any of the eigenvector components, see equation (17b)
p	pressure
$\tilde{p}$	disturbance pressure
Pr	Prandtl number
q	exponent in the density relation of Gebhart and Mollendorf [18]
R	density extremum parameter, see equation (1)
$S(\eta)$	nondimensional disturbance temperature amplitude function
$\bar{S}(y)$	disturbance temperature amplitude function
T	temperature
U	characteristic velocity
u, v	velocity components
$\tilde{u}, \tilde{v}$	disturbance velocity components
$W(\eta)$	nondimensional local buoyancy force
x, y	coordinates
Z	coefficient, see equation (12c)
Z_0	coefficient in the stability equation, $\delta q\lvert\theta_b - R\rvert^{q-1}(\theta_b - R)/\lvert\theta_b - R\rvert$.

Greek symbols

α	complex wave number, $\alpha_R + i\alpha_I$, $\alpha = \alpha_R$ for neutral stability
α^*	α at G_{cr}
α_T	thermal expansion coefficient in the density relation of Gebhart and Mollendorf [18], $(^\circ C)^{-q}$
β	disturbance frequency
δ	$+1.0$ for upflow, -1.0 for downflow
δ_T	thermal boundary layer (in Fig. 2)
$\eta(x, y)$	similarity variable
$\eta_{P.I.j}$	points of inflection in the velocity profile $(j = 1, 2)$
$\theta(\eta)$	nondimensional temperature, $(T - T_\infty)/(T_0 - T_\infty)$
$\tilde{\theta}$	disturbance temperature
λ	wavelength
ν	kinematic viscosity
ρ	density
τ	time
$\Phi(\eta)$	nondimensional disturbance velocity amplitude function
$\bar{\Phi}(y)$	disturbance velocity amplitude function
ϕ	eigenvector, see equation (13)
$\psi(x, y)$	stream function
$\tilde{\psi}(x, y, \tau)$	disturbance stream function.

Subscripts

b	base flow property
m	at the extremum condition
I	imaginary
0	surface condition
R	real
∞	at ambient condition.

Other symbols

-	dimensional quantity
~	disturbance quantity.

$T_m = 4.029325^\circ C$ at 1 bar), a considerable buoyancy force reversal arises across the thermal boundary layer. To efficiently predict the resulting subtle flow patterns, the following density extremum parameter was defined by Gebhart and Mollendorf [10]:

$$R = \frac{T_m - T_\infty}{T_0 - T_\infty} \tag{1}$$

where T_0 and T_∞ are the temperature of the isothermal surface and the temperature of the ambient medium (cold pure water), respectively.

The analysis of the steady-state flows in the presence of buoyancy force reversals in the range of $0 < R < 0.5$ is complex. To save space we do not discuss these matters in detail here, although they are important in relation to our stability analysis; but we refer

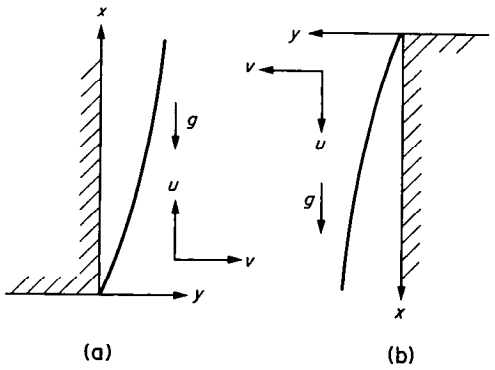

FIG. 1. The coordinate system: (a) upflow; (b) downflow.

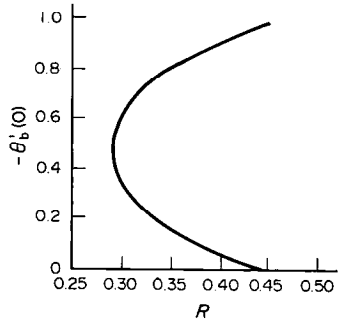

FIG. 3. Details of variation of heat transfer rate $-\theta_b'(0)$ with R in the region $0.29181 \leqslant R \leqslant 0.45402$ (largely downflow). From El-Henawy *et al.* [4].

to Wilson and Vyas [11] and Carey and Gebhart [12] for experimentally observed flows and to Gebhart and Mollendorf [10], Carey *et al.* [13], and El-Henawy *et al.* [4] for the representation of similarity solutions for such flows.

This study is concerned principally with the presentation, for various values of the density extremum parameter R in the range of $0.29181 \leqslant R \leqslant 0.50$, of numerical results that, it is hoped, predict realistic physical conditions for neutral stability for the base flows generated by natural convection adjacent to a vertical, isothermal plate (as seen in Fig. 1) in cold pure water. The hydrodynamic stability of these base flows is of special interest, since under these conditions inside buoyancy force reversals (such as those seen in Fig. 2) exert a strong influence upon the flow and the multiple steady-state solutions of El-Henawy *et al.* [4] are predicted to exist.

It is convenient to distinguish among the multiple steady-state solutions as follows. For the two steady-states which exist at the same R for the flow (as seen in Fig. 3), in the range $0.29181 \leqslant R \leqslant 0.45402$, the solution that has a higher heat flux ($-\theta_b'(0)$) is called the upper-branch solution and the other, with a lower heat flux, is called the lower-branch solution.

The influence of these multiple solutions on instability and transition may be considerable. The main results of this study show this to be the case.

The numerical study of the stability of the base flows for non-Boussinesq situations is difficult. Difficulty exists partly because the base flow itself is sensitive to buoyancy force reversal via the nonlinear buoyancy force term in the mathematical model as discussed in El-Henawy *et al.* [4]. An additional significant difficulty may come from the presence of a singularity in the linear stability equations (the so-called Orr–Sommerfeld equations) as used by Qureshi [14] and Higgins [15]; see also, Higgins and Gebhart [16] and Qureshi and Gebhart [17]. Thus, we reformulated the stability equations to render them non-singular. This is done in Section 2.2.

Secondly, because the system of stability equations is a moderately stiff two-point boundary-value eigenvalue problem, the method of simple shooting used previously in refs. [5, 6] is unsuccessful owing to the serious impact of accumulated integration error and the inaccuracy resulting from superpositions. Thus, this system must be solved by a state-of-the-art, two-point boundary-value problem solving code. A computer code, COLSYS [3], based on orthogonal collocation was used for this purpose.

Due to the difficulties mentioned above, although

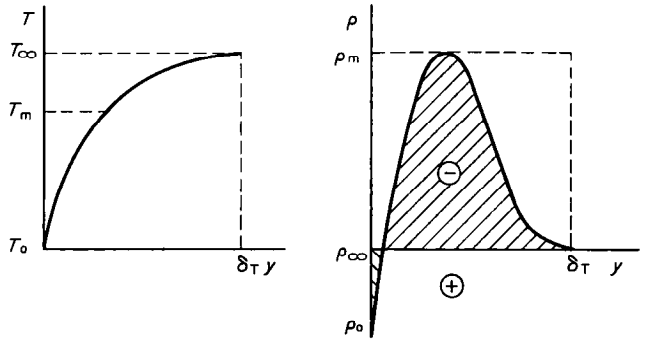

FIG. 2. For $R = 0.5^-$, an inside buoyancy force reversal appears.

knowledge of stability of the base flow (in the range $0 < R < 0.5$) is important in applications, the previous numerical study of Higgins [15] yields limited information concerning only one simple case: $R = 0.4$ (the upper-branch solution only).

Qureshi [14] first utilized the density relation of Gebhart and Mollendorf [18] to calculate the buoyancy effect in a study of hydrodynamic stability for flow adjacent to vertical uniform heat flux and isothermal surfaces in ambient water at the density extremum temperature, i.e. $R = 0$ (see also ref. [17] for stability results at two different levels of pressure).

Higgins [15] solved the stability equations for a vertical isothermal surface for $R = 0.4$ (upper-branch solution), and for several values of R with $1.0 \leqslant R \leqslant 8.0$ and $R = -0.5$ (see also ref. [16]). All of these numerical results were obtained via simple shooting.

The experimental studies by Higgins and Gebhart [19] for an isothermal surface at $R = 0.0$, 0.12, and 0.4 and of Qureshi and Gebhart [20] for a uniform heat flux surface at $R = 0$ in cold water indicate that the density extremum behavior was found to delay transition, compared to results in water at room temperature. Also, they found that the selective amplification mechanism is less sharp for cold water than for water at room temperature.

El-Henawy *et al.* [21] studied the '*configurational stability*' of the multiple steady-state solutions found by El-Henawy *et al.* [4]. They found that the lower-branch solutions are less stable than the upper-branch solutions for $R > 0.29181$. This agrees with the present study. However, the weakest aspect of their configurational stability analysis is that it could not provide important information such as the point of instability (i.e. the critical Grashof number) and the frequencies and wave numbers of unstable disturbances. Thus, the need for the present study as an analysis of classical hydrodynamic stability is evident.

In addition, El-Henawy *et al.* [21] were able to numerically determine the stability of solutions near $R = 0.15180$, while we were not. Their approach has the advantage relative to ours of ease of numerical calculations of the real eigenvalues and eigenfunctions.

The present numerical study includes neutral stability results for the region of the base flows corresponding to $0.29181 \leqslant R \leqslant 0.50$ for $Pr = 11.6$. In particular, neutral stability curves are obtained at $R = 0.30$, 0.32, and 0.34 for the two steady-states, corresponding to the upper- and lower-branch solutions which were found by El-Henawy *et al.* [4]. Also, portions of the '*noses*' of the stability curves are computed for the single solution at $R = 0.29181$, and for the upper-branch solution only at $R = 0.38$, and rather more complete stability curves are obtained for the upper-branch solutions at $R = 0.36$, 0.40, and 0.50.

It will be seen that a flow in the range $0.29181 \leqslant R \leqslant 0.50$ is always stable for a disturbance whose dimensionless frequency parameter B is greater than 0.4914 (i.e. if $|T_0 - T_\infty| = 4°C$, and whose corresponding physical frequency $f > 0.16$ Hz). It will also be shown that increasing the heat transfer rate of base flows ($-\theta_b'(0)$) causes the corresponding critical Grashof number to increase systematically.

2. FORMULATION OF THE GOVERNING EQUATIONS

2.1. *Base flow*

The similarity equations for steady laminar base flows (with the coordinate definitions in Fig. 1) are well known [4, 10, 13]. To formulate them the following nondimensional quantities were used: η (a similarity variable), $f_b(\eta)$ (stream function), and $\theta_b(\eta)$ (temperature), where

$$\eta = \frac{yG}{4x}, \quad \psi_b(x, y) = \nu G f_b(\eta), \quad \theta_b(\eta) = \frac{T - T_\infty}{T_0 - T_\infty} \tag{2a}$$

and

$$G = 4(\tfrac{1}{4}Gr(x))^{1/4}, \quad Gr(x) = \frac{gx^3}{\nu^2}\alpha_T|T_0 - T_\infty|^q. \tag{2b}$$

Here α_T and q are the thermal expansion coefficient and exponent, respectively, from the density relation of Gebhart and Mollendorf [18]. For conditions at 1 bar pressure and no salinity, $\alpha_T = 9.297173 \times 10^{-6}(°C)^{-q}$ and $q = 1.894816$. The base flow buoyancy force term is:

$$g(\rho_\infty - \rho) = \delta g \rho_m \alpha_T |T_0 - T_\infty|^q (|\theta_b - R|^q - |R|^q) \tag{3}$$

with $\delta = +1$ for largely upward flow and $R \leqslant 0.15180$, $\delta = -1$ for largely downward flow and $R \geqslant 0.29181$. Here ρ_m denotes the extremum density.

The equations for the base flow in similarity form are:

$$f_b''' + 3f_b f_b'' - 2f_b'^2 + \delta(|\theta_b - R|^q - |R|^q) = 0 \tag{4a}$$

$$\theta_b'' + 3Pr\, f_b \theta_b' = 0 \tag{4b}$$

with boundary conditions

$$f_b'(0) = f_b(0) = 1 - \theta_b(0) = f_b'(\infty) = \theta_b(\infty) = 0; \tag{5}$$

see Gebhart and Mollendorf [10]. $Pr = 11.6$ is the Prandtl number for cold pure water.

Here we only consider downward flows in the range $0.29181 \leqslant R \leqslant 0.50$, where inside buoyancy force reversals occur. The boundary-value problem (4a,b)–(5) was solved on intervals $[0, \eta_\infty]$ with $\eta_\infty = 60$–150 by using two computer codes: COLSYS [3] and BOUNDS [22]. To generate the families of solutions, the continuation schemes of El-Henawy *et al.* [4] were employed. Examples of dimensionless vertical velocity and temperature profiles for multiple, steady-state base flows are given in Figs. 4 and 5. Also, the profiles

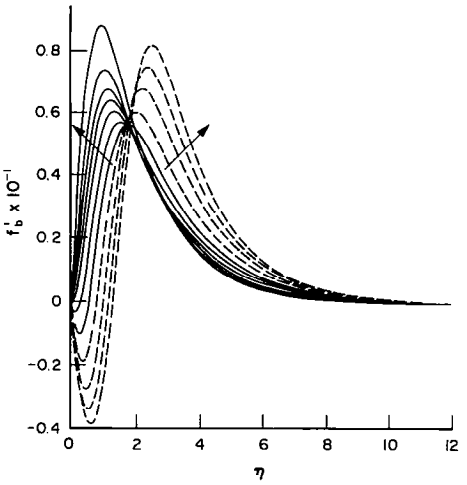

FIG. 4. Dimensionless vertical velocity component $f'_b(\eta)$. For the upper-branch solutions (——), the arrow indicates increasing R for $R = 0.29181$, 0.30, 0.32, 0.34, 0.36, 0.40, and 0.50. For the lower-branch solutions (···), the arrow indicates increasing R for $R = 0.30$, 0.32, 0.34, and 0.36.

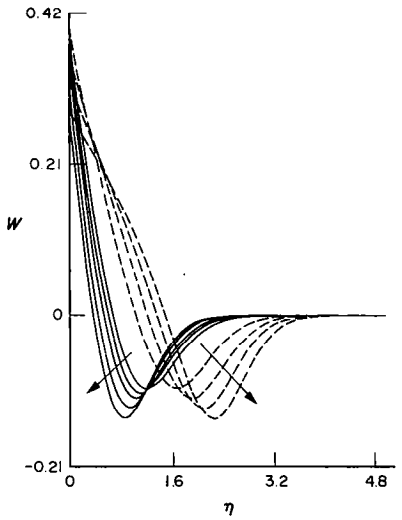

FIG. 6. Distribution of local buoyancy force $W(\eta)$. For the upper-branch solutions (——), the arrow indicates increasing R for $R = 0.30$, 0.31, 0.32, 0.34, and 0.36. For the lower-branch solutions (···), the arrow indicates increasing R for $R = 0.30$, 0.32, 0.34, and 0.36.

of local buoyancy force $W = |\theta_b - R|^q - |R|^q$ are shown in Fig. 6.

The heat transfer rates $-\theta'_b(0)$ of the upper- and lower-branch base flows in Fig. 3, each of which has the same R, q, and Pr, may differ by as much as a factor of ten or more. The lower-branch solution has thicker thermal and hydrodynamic boundary layers and a more vigorous (reversed) flow than does the upper-branch solution. For upper-branch solutions, as R decreases from 0.50 to 0.29181, the upward buoyancy force near $\eta = 0$ increases and the shear stress at the surface $f''_b(0)$ decreases and becomes negative. For the lower-branch solutions, the upward buoyancy force causes an inside flow reversal, which becomes steadily stronger as R increases from 0.29181 to 0.45 (see Figs. 4 and 6).

Due to the effects of inside buoyancy force reversals, all the base flows corresponding to $0.29181 \leqslant R < 0.50$ have two points of inflection in their velocity profiles. Also, as the heat transfer rate $-\theta'_b(0)$ increases from near 0.0 to above 1 and, simultaneously, the shear force $f''_b(0)$ increases, we find that the two points of inflection in the velocity profiles shift towards $\eta = 0$. The shift of the two inflection points might increase the limit of stability of the flow, just as in forced flow problems [23]. This point will be discussed later.

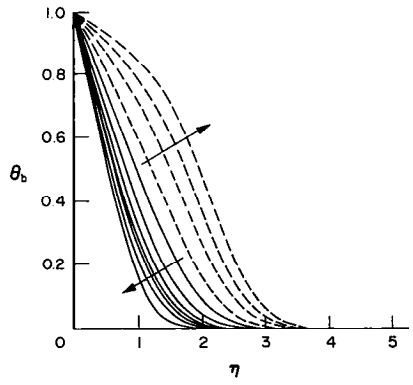

FIG. 5. Normalized temperature $\theta_b(\eta)$. For the upper-branch solutions (——), the arrow indicates increasing R for $R = 0.29181$, 0.30, 0.32, 0.34, 0.36, 0.40, and 0.50. For the lower-branch solutions (···), the arrow indicates increasing R for $R = 0.30$, 0.32, 0.34, and 0.36.

2.2. *The linear stability equations*

A linear stability analysis is employed: we assume perturbations that are small two-dimensional disturbances of the vertical velocity u, horizontal velocity v, temperature θ and pressure p; namely, $u = u_b(x, y) + \tilde{u}(x, y, \tau)$ and analogously for v, p and θ. The disturbance vector $(\tilde{u}, \tilde{v}, \tilde{p}, \tilde{\theta})$ may be decomposed into a periodic series. To handle the linear stability problem mathematically, the following '*modes*' of the stream, temperature and pressure functions, $\tilde{\psi}$, $\tilde{\theta}$ and $\tilde{p}$, are postulated:

$$\tilde{\psi} = \bar{\Phi}(y)\, e^{i(\bar{\alpha}x - \bar{\beta}\tau)} \tag{6a}$$

$$\tilde{\theta} = \bar{S}(y)\, e^{i(\bar{\alpha}x - \bar{\beta}\tau)} \tag{6b}$$

$$\tilde{p} = \bar{H}(y)\, e^{i(\bar{\alpha}x - \bar{\beta}\tau)} \tag{6c}$$

where for neutral stability, $\bar{\alpha}$ and $\bar{\beta}$ may be expressed as $\bar{\alpha} = 2\pi/\lambda$, $\bar{\beta} = 2\pi f$. The quantities $\bar{\alpha}$ and $\bar{\beta}$ are the wave number and frequency, respectively.

The disturbance quantities are normalized in the following manner, where D and U are the characteristic length and velocity:

$$\Phi(\eta) = \frac{\bar{\Phi}(y)}{UD}, \quad S(\eta) = \frac{\bar{S}(y)}{T_0 - T_\infty}, \quad H(\eta) = \frac{\bar{H}(y)}{\rho U^2},$$

$$\alpha = \bar{\alpha}D, \quad \beta = \frac{\bar{\beta}D}{U}, \quad D = \frac{4x}{G}, \quad U = \frac{\nu G^2}{4x}. \tag{7}$$

In our formulation of the linear stability equations, the buoyancy force disturbance is given special consideration. The perturbed buoyancy force term is

$$g(\rho_\infty - \rho) = \delta g \rho_m \alpha_T |T_0 - T_\infty|^q (|\theta_b - R + \tilde{\theta}|^q - |R|^q). \tag{8}$$

Its conventional Taylor series expansion about θ_b can be written as

$$|\theta_b - R + \tilde{\theta}|^q = q \frac{(\theta_b - R)}{|\theta_b - R|} |\theta_b - R|^{q-1} \tilde{\theta} + o(\tilde{\theta}) \tag{9}$$

where $o(\tilde{\theta})/\tilde{\theta} \to 0$ as $\tilde{\theta} \to 0$.

Thus, the net first approximation to the perturbation of the buoyancy is $Z_0\tilde{\theta}$, where

$$Z_0 \equiv \delta q \frac{(\theta_b - R)}{|\theta_b - R|} |\theta_b - R|^{q-1}.$$

The postulated disturbances are substituted into the complete time-dependent Navier–Stokes and energy equations. The usual parallel flow approximation is applied and the higher order disturbance terms are neglected. Some aspects of the x-dependence of U and D are neglected. This has been discussed by Hieber and Gebhart [6]. The pressure disturbance terms H and H' are retained to avoid a singularity. (If the pressure components H and H' are not retained by us in the x- and y-momentum disturbance equations, then we must differentiate the buoyancy force $W(\theta_b, R) \equiv |\theta_b - R|^q - |R|^q$ to eliminate the pressure disturbance terms from the system and to linearize it [15]. However, since θ_b decreases monotonically from 1 to 0 as η goes from 0 to ∞ and since $q = 1.894816$, $\partial^2 W(\theta_b, R)/\partial\theta_b^2$ has a singularity for $\theta_b = R$, which we have avoided.) Our nonsingular Orr–Sommerfeld equations for buoyancy-induced flow are:

x-momentum

$$(f_b' - c)\Phi' - f_b''\Phi = -H + \frac{1}{i\alpha G}(\Phi''' - \alpha^2\Phi' + Z_0 S) \tag{10a}$$

y-momentum

$$(f_b' - c)\Phi = -\frac{H'}{\alpha^2} + \frac{1}{i\alpha G}(\Phi'' - \alpha^2\Phi) \tag{10b}$$

energy

$$(f_b' - c)S - \theta_b'\Phi = \frac{1}{i\alpha G\, Pr}(S'' - \alpha^2 S) \tag{10c}$$

where $c = \beta/\alpha$, and $\delta = +1.0$ for upflow and -1.0 for downflow.

We next specify the boundary conditions. If the plate has sufficiently large thermal capacity, $\tilde{\theta}$ must be zero at the isothermal surface, i.e. $\tilde{\theta}(0) = 0$. Evidently, at a large distance out ($y \to \infty$), the disturbance quantities $\tilde{p}$, $\tilde{u}$, and $\tilde{\theta}$ must be zero. Therefore, the nondimensional boundary conditions are:

$$\Phi(0) = \Phi'(0) = S(0) = \Phi'(\infty) = S(\infty) = H(\infty) = 0. \tag{11}$$

The foregoing equations (10a–c) and (11) constitute a complex-valued, sixth-order, linear system of homogeneous differential equations. The eigenvalues of the system are the nondimensional wave number α and frequency β. The ratio β/α is called the wave speed c. If the terms $H(\eta)$ and $H'(\eta)$ are eliminated from the system, then these stability equations are the same as the conventional ones of Qureshi [14] and Higgins [15] (see also refs. [16, 17]), but our boundary conditions are slightly different.

3. SOLVING THE LINEAR STABILITY EQUATION

Previous investigators solved their linear stability equations by simple shooting from $\eta = \eta_\infty$, where one matches the asymptotic solution valid as $\eta \to \infty$ to $\eta = 0$, and one seeks to satisfy the conditions that apply at $\eta = 0$ [5, 6, 14, 15]. However, we found simple shooting to be sufficient only for obtaining initial guesses for the solutions of Qureshi [14] and Higgins [15]. We obtained our results primarily by using the collocation (B-spline) code COLSYS [3]. To guide the simple shooting integrations we used three sets of independent integrals:

$$\Phi_1 = e^{-\alpha\eta}, \quad S_1 = 0, \quad H_1 = -\beta e^{-\alpha\eta} \tag{12a}$$

$$\Phi_2 = e^{-\alpha_2\eta}, \quad S_2 = 0, \quad H_2 = 0 \tag{12b}$$

$$\Phi_3 = -\frac{\alpha_3 Z}{(\alpha c G)^2 Pr(Pr-1)} e^{-\alpha_3\eta}, \quad S_3 = e^{-\alpha_3\eta},$$

$$H_3 = -\frac{Z}{c Pr\, G^2} e^{-\alpha_3\eta} \tag{12c}$$

where

$$\alpha_2^2 = \alpha^2 - i\alpha c G, \quad \alpha_3^2 = \alpha^2 - i\alpha\, Pr\, c G,$$

$$Z = -\delta \frac{R}{|R|} q |R|^{q-1}.$$

Here the subscripts 1, 2, and 3 correspond to the inviscid, the viscous uncoupled and the viscous coupled solutions.

The eigenvectors are expressed as the linear combination:

$$\boldsymbol{\phi} = c_1\boldsymbol{\phi}_1 + c_2\boldsymbol{\phi}_2 + c_3\boldsymbol{\phi}_3 \tag{13}$$

where

$$\boldsymbol{\phi} = \begin{bmatrix} \Phi_i \\ S_i \\ H_i \end{bmatrix} \quad (i = 1, 2, 3)$$

and where c_1, c_2 and c_3 are complex constants to be determined. The constant c_1 is chosen as $c_1 = 1 + 1i$ to fix the scale arbitrarily.

To reduce error propagation and to avoid the inaccuracies inherent in simple shooting, the two-point boundary-value-problem solver COLSYS was used. With it we were able to compute accurate numerical solutions of the stability equations in the range

$0.29181 \leqslant R \leqslant 0.5$. These cannot be found by simple shooting.

To generate families of solutions, two different *ad hoc* schemes were used. These are described below. Since there is no simple way to normalize the solutions of the eigenvalue problem (10a–c) and (11) which has all homogeneous boundary conditions, an alternative must be found to avoid the trivial solution.

The first scheme, which succeeded, was to replace the boundary condition $\Phi_i'(0) = 0$ by

$$\Phi_R(\eta_\infty) = k_1 \tag{14}$$

with $10^{-9} \leqslant k_1 \leqslant 10^{-6}$ or, alternatively, by

$$S_R'(0) = k_2 \tag{15}$$

with $0.04 \leqslant k_2 \leqslant 0.2$. Additionally, the condition $\Phi_R'(0) = 0$ is replaced by $\Phi_i(\eta_\infty) = 0$. (The reason for choosing $\Phi_i(\eta_\infty)$ as zero, instead of $\Phi_R(\eta_\infty)$, is that $|\Phi_i(\eta)|$ decreases more rapidly as $\eta \to \eta_\infty$ for moderate values of α and β than does $|\Phi_R(\eta_\infty)|$. For extremely small α and β (i.e. on the lower portion of the neutral stability curve), since $|\Phi_R(\eta_\infty)| \ll |\Phi_i(\eta_\infty)|$ as $\eta \to \eta_\infty$, $\Phi_i(\eta_\infty)$ is chosen as nonzero and $\Phi_R(\eta_\infty) = 0$.) It is the finiteness of the intervals of integration (finiteness of η_∞) that makes these choices necessary.

The computing procedure employed to use the orthogonal collocation code COLSYS for obtaining the neutral stability curve is quite similar to that employed in simple shooting. For a given value G, one guesses a pair of eigenvalues α and β. One then solves the boundary-value problem (10a–c) and (11) with the modified boundary condition (14) or (15), replacing $\Phi_i'(0) = 0$, using COLSYS, and one iterates by adjusting the values of α and β until the boundary conditions $\Phi_R'(0) = \Phi_i'(0) = 0$ are satisfied with $|\Phi_R'(0)| + |\Phi_i'(0)| \leqslant 10^{-6}$.

The second scheme is to add the trivial differential equations

$$\alpha' = 0, \quad \beta' = 0 \tag{16}$$

to the system (10a–c) and to impose two nonzero conditions $S_R'(0) = k_2$ and $S_i'(0) = k_3$ with $0.05 \leqslant |k_3| \leqslant 1.0$ or, alternatively, $\Phi_R(\eta_\infty) = k_1$ and $S_R'(0) = k_2$ in addition to (11). This scheme yields exact numerical solutions of the original eigenvalue problem (10a–c), (11) and (16). However, to get it to work accurate initial guesses are required.

When we used the first scheme, we insisted that, for a solution to be accepted, the following criteria were all met:

$$\min_{0 \leqslant \eta \leqslant \eta_\infty} \left(\frac{|\Phi_R'(0)|}{|\Phi_R'(\eta)|}, \frac{|\Phi_i'(0)|}{|\Phi_i'(\eta)|} \right) \leqslant 10^{-4} \tag{17a}$$

$$\max \left(\frac{|\Phi_R'(0)|}{M}, \frac{|\Phi_i'(0)|}{M} \right) \leqslant 10^{-7} \tag{17b}$$

where M is the largest magnitude of any of the eigenvector components (i.e. Φ, Φ', Φ'', S, S', H) on $0 \leqslant \eta \leqslant \eta_\infty$. In addition, the error estimates given on output by COLSYS are less than 10^{-4}.

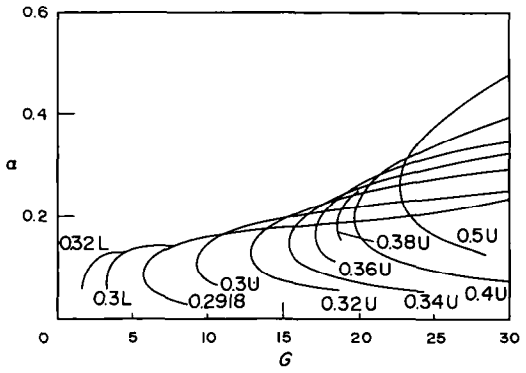

FIG. 7. Portions of computed neutral stability curves in the (G, α) plane for upper- and lower-branch solutions.

The second scheme was used for the purpose of verification and improvement of the numerical results, which were obtained by the first scheme.

4. NUMERICAL RESULTS ON NEUTRAL STABILITY

The critical Grashof number G_{cr} is the smallest Grashof number on a neutral stability curve in the (G, β) (or (G, B)) or (G, α) plane. For $G < G_{cr}$ any small disturbance decays, whereas for $G > G_{cr}$ at least some disturbances are amplified. Since there is one neutral stability curve corresponding to each $(R, -\theta_b'(0))$, we can consider G_{cr} to be a function of R on the upper branch or the lower branch of the bifurcation curves shown in Fig. 3.

We obtained neutral stability results that satisfy the criteria for accuracy (17a,b) for several R values in the range $0.29181 \leqslant R \leqslant 0.50$. In particular, for $R = 0.30$ and 0.32, we obtained rather complete neutral stability curves for the two steady-states. For $R = 0.34$ the neutral stability curve for the upper-branch solution is easily computed, but for $R = 0.34$, at lower values of G (i.e. $G < 12$) the computation of the neutral stability curve corresponding to the lower-branch solution is too sensitive to carry it out with confidence. In addition, we computed portions of the '*nose*' of the neutral stability curves for the single solution at $R = 0.29181$, and for the upper-branch solution only at $R = 0.38$. Rather more complete stability curves are computed for the upper-branch solutions at $R = 0.36$, 0.40, and 0.50. Examples of these results are shown in Figs. 7–19 and Tables 1–3.

Some of our numerical results on stability are presented in the (G, B) plane, where

$$B = \beta G^{1/3} = \frac{2\pi f}{\nu} \left(\frac{g}{\nu^2} \alpha_T |T_0 - T_\infty|^q \right)^{-2/3}. \tag{18}$$

This parameter B has no x dependence, it is proportional to the physical frequency f. Constant frequency paths for G are horizontal straight lines in the stability plane (G, B); see Figs. 9, 12 and 13. Also, some of our neutral stability results are presented in

Table 1. Values of G_{cr}, B^*, α^*, and A_{max} for various values of R

R	G_{cr}	B^*	α^*	A_{max}
0.50U	22.81	0.0828	0.2483	0.1909
0.40U	19.62	0.0525	0.1899	0.1478
0.38U	18.48	0.0476	0.1810	—
0.36U	17.06	0.0411	0.1652	0.1314
0.34U	15.23	0.0347	0.1477	0.1246
0.32U	12.81	0.0280	0.1277	0.1182
0.30U	9.19	0.0209	0.1030	0.1125
0.29181	5.69	0.0161	0.0821	0.1090
0.30L	3.16	0.0146	0.0774	0.1058
0.32L	1.50	0.0127	0.0583	0.1022
0.34L	—	—	—	0.0991

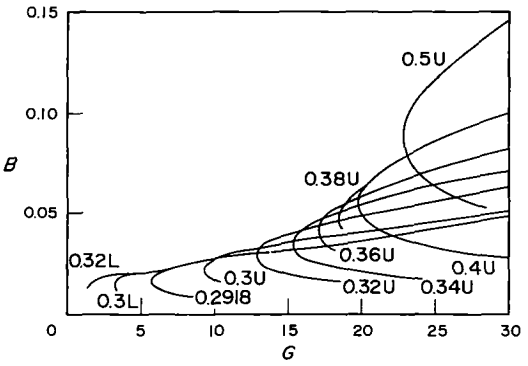

FIG. 9. Portions of computed neutral stability curves in the (G, B) plane for upper- and lower-branch solutions.

terms of a parameter A, which has no x dependence, where

$$A = \alpha G^{-1/3} = \frac{2\pi}{\lambda}\left(\frac{g}{\nu^2}\alpha_T|T_0 - T_\infty|^q\right)^{-1/3}. \quad (19)$$

The parameter A is proportional to the physical wave number $2\pi/\lambda$. Table 1 shows the maximum value of A, A_{max}, at various values of R.

If $|T_0 - T_\infty|$ is fixed (i.e. T_0 and T_∞ are allowed to change equally. One can imagine that one can, within certain limits, vary the temperature T_0 of the vertical plate), a plot in the (G, B) plane (also the (G, α) and (G, β) planes), or a table is useful in quantitatively analyzing the linear stability results. The quantity $|T_0 - T_\infty|$ is assumed to be constant in the following discussion.

The critical Grashof number G_{cr} steadily decreases from $G_{cr} = 22.81$ to 5.69 as R decreases from $R = 0.5$ to 0.2918 for flows corresponding to upper branch solutions. This is observed in Figs. 7–9 and Table 1. Recall that for the region of largely downward base flow ($0.29181 \leqslant R < 0.50$), inside buoyancy force reversals affect transport characteristics of base flows. The upward buoyancy force near $\eta = 0$ steadily increases as R decreases (i.e. the inside buoyancy force reversals become stronger). At the same time the heat flux of base flows $-\theta_b'(0)$ consistently decreases from above 1.0 at $R = 0.5$ to 0.4940 at $R = 0.29181$. Thus, decreasing the heat flux of base flows causes the corresponding point of instability G_{cr} to decrease. In other words, increases in the magnitude of inside buoyancy force reversal cause the corresponding flows to become significantly more unstable.

Table 2. Crossing points of the upper- and lower-branch solutions in the (G, α) or (G, A) plane

R	$G_{\alpha 1}$	$G_{\alpha 2}$	$G_{\alpha 3}$	α_1	α_2	α_3	A_1	A_2	A_3
0.30	10.05	29.17	66.90	0.1457	0.1518	0.4271	0.0675	0.0818	0.105
0.32	12.82	36.19	47.30	0.1287	0.3184	0.3640	0.0550	0.0963	0.101
0.34	15.28	—	—	0.1413	—	—	0.0569	—	—

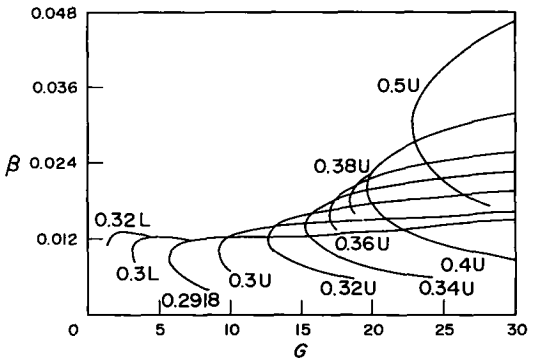

FIG. 8. Portions of computed neutral stability curves in the (G, β) plane for upper- and lower-branch solutions.

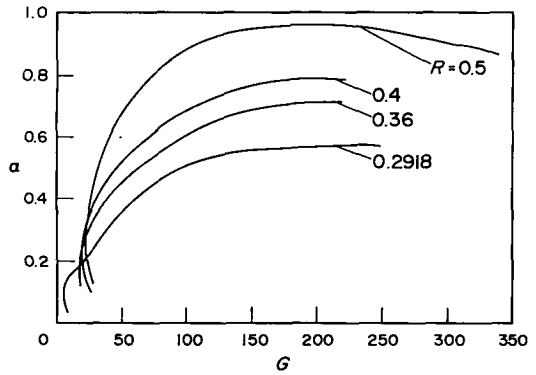

FIG. 10. Computed neutral stability curves in the (G, α) plane for upper-branch solutions.

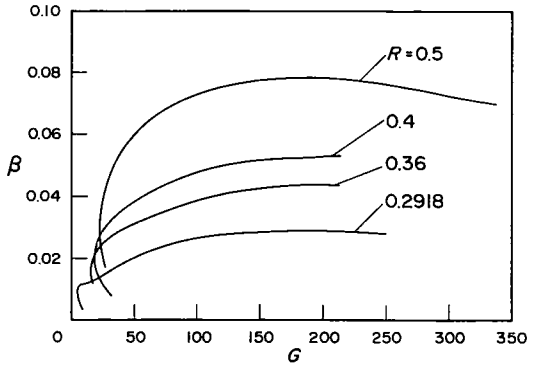

FIG. 11. Computed neutral stability curves in the (G, β) plane for upper-branch solutions.

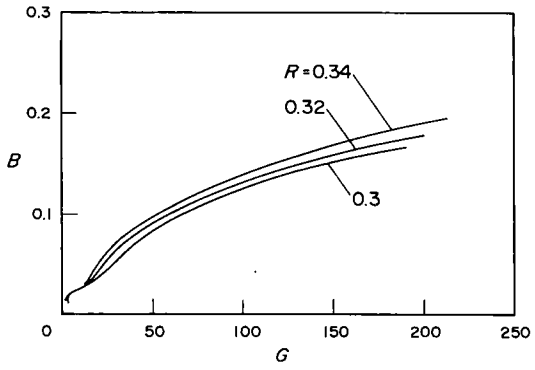

FIG. 13. Computed neutral stability curves in the (G, B) plane for lower-branch solutions.

As the parameter R or $-\theta_b'(0)$ is decreased, the shapes of the corresponding neutral stability curves in the stability planes systematically change. Not only G_{cr} but also the quantities α^* and B^*, which are the values of α and β at G_{cr}, respectively, decrease significantly, as R or $-\theta_b'(0)$ decreases. The 'nose' of a neutral stability curve shifts toward the origin of the (G, B) (or (G, B)) and (G, α) planes and its shape becomes sharper as R decreases. This implies that the lower limits of unstable disturbance frequencies and wave numbers are expected to decrease as R decreases from 0.50 to 0.29181.

As seen from Figs. 11 and 12, the upper part of the neutral stability curve in the (G, B) (or (G, β)) plane corresponding to $R = 0.50$ is above that of the other curves. Evidently, the upper limit of unstable frequency for the flows is bounded by the value of $B_{max} = 0.4914$ at $R = 0.50$. In other words, a flow (in the range $0.29181 \leqslant R \leqslant 0.50$) is always stable for the disturbance whose frequency, in terms of B, is greater than 0.4914. The physical frequency corresponding to $B = 0.4914$ is 0.16 Hz if $|T_0 - T_\infty| = 4°C$ and 0.38 Hz if $|T_0 - T_\infty| = 8°C$, for $(T_0 + T_\infty)/2 = 4°C$. It is expected that the upper limit of frequency with respect to R decreases as R decreases. Also, it is observed from Table 1 that the upper limit of wave number A_{max} decreases considerably as R or $-\theta_b'(0)$ decreases (see Fig. 10). The value of $A_{max} = 0.1909$ at $R = 0.50$ bounds the upper limit of wave number of unstable disturbances for flows (in the range $0.29181 \leqslant R \leqslant 0.50$). For $(T_0 + T_\infty)/2 = 4°C$, the physical wavelength corresponding to $A = 0.1909$ is 4.1 cm if $|T_0 - T_\infty| = 4°C$ and 2.65 cm if $|T_0 - T_\infty| = 8°C$. Thus, the flows corresponding to upper-branch

Table 3. Crossing points of the upper- and lower-branch solutions in the (G, β) or (G, B) plane

R	$G_{\beta 1}$	$G_{\beta 2}$	$G_{\beta 3}$	β_1	β_2	β_3	B_1	B_2	B_3
0.30	9.64	24.86	74.71	0.0119	0.0157	0.0251	0.0253	0.0458	0.106
0.32	12.83	24.00	63.92	0.0122	0.0187	0.0260	0.0284	0.0539	0.104
0.34	15.29	30.20	41.72	0.0147	0.0230	0.0252	0.0365	0.0717	0.087

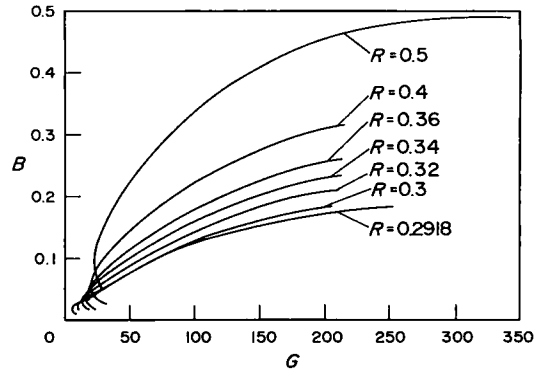

FIG. 12. Computed neutral stability curves in the (G, B) plane for upper-branch solutions.

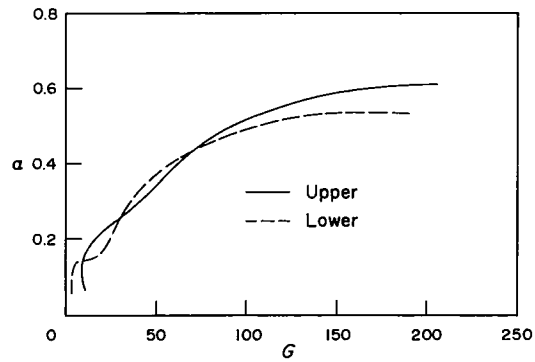

FIG. 14. Computed neutral stability curves in the (G, α) plane for the upper- and lower-branch solutions at $R = 0.30$.

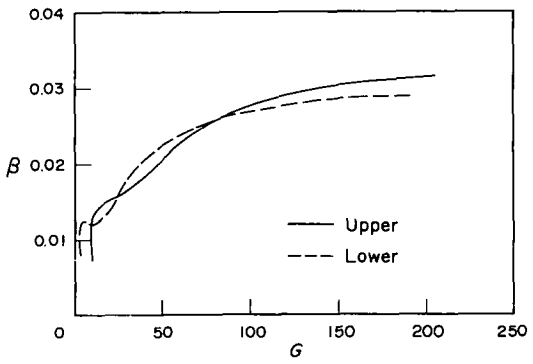

FIG. 15. Computed neutral stability curves in the (G, β) plane for the upper- and lower-branch solutions at $R = 0.30$.

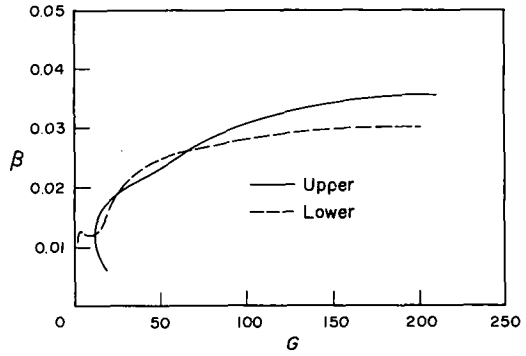

FIG. 17. Computed neutral stability curves in the (G, β) plane for the upper- and lower-branch solutions at $R = 0.32$.

solutions are more unstable for lower frequencies and wave numbers as R (or $-\theta_b'(0)$) decreases.

If we consider flows corresponding to lower-branch solutions, the characteristics of their neutral stability are quite similar to those of flows corresponding to upper-branch solutions. However, the behavior of the upper limit of frequencies with respect to $-\theta_b'(0)$ is quite different for these two kinds of solutions. As seen from Fig. 13, the value of B, at fixed G for $G \geqslant 20$, corresponding to the upper portion of the neutral stability curves, consistently increases as $-\theta_b'(0)$ decreases (or R increases) for lower-branch solutions. It is conjectured that the frequencies represented on neutral stability curves increase as R increases. However, the values of B^* and α^* (B and α at G_{cr}) slightly decrease as R increases (see Table 1). Thus, the flow corresponding to a lower-branch solution is expected to be unstable for a wider range of frequencies as R increases. At the same time, one expects the range of unstable wave numbers to be reduced.

If we consider both flows corresponding to upper- and lower-branch solutions, we find that the difference in G_{cr}, B^* and A_{max} between the value corresponding to the upper-branch solution and the value corresponding to the lower-branch solution at the same R significantly increases as R increases from $R = 0.29181$ toward $R = 0.34$. For example, the difference in G_{cr} is 6.03 at $R = 0.30$ and 11.31 at $R = 0.32$. However, for R fixed in the range $0.30 \leqslant R \leqslant 0.34$, the neutral stability curve in the stability planes for a lower-branch solution crosses the curve for the corresponding upper-branch solution at one to three points; see Figs. 14–19 and Tables 2 and 3. The interpretation of these curves is complicated due to their crossing each other. This will be discussed in Section 5.

Figures 20 and 21 show the real and imaginary parts of the eigenvector components (Φ, Φ', S, H) which satisfy the accuracy criteria (17a,b), corresponding to the '*noses*' of neutral stability curves at $R = 0.34$ and 0.40. In these figures, the eigenvectors are normalized by the maximum value of the components. The shapes of the components of the eigenvectors change dramatically as R changes in response to the change in strength of inside buoyancy force reversals.

5. DISCUSSION AND CONCLUSION

The previous section presented the major new findings in terms of stability planes by plotting nondimensional wavelength and frequency versus modified Grashof number. The concept of constant physical frequency was discussed in the previous section. This concept is important in interpreting the physical

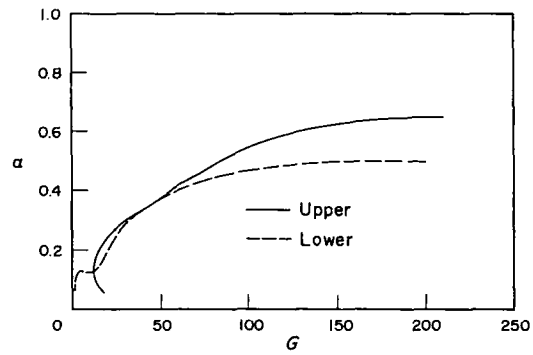

FIG. 16. Computed neutral stability curves in the (G, α) plane for the upper- and lower-branch solutions at $R = 0.32$.

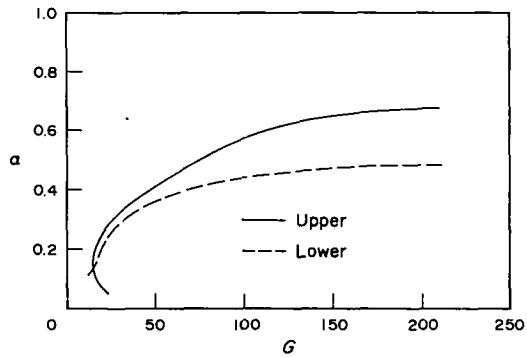

FIG. 18. Computed neutral stability curves in the (G, α) plane for the upper- and lower-branch solutions at $R = 0.34$.

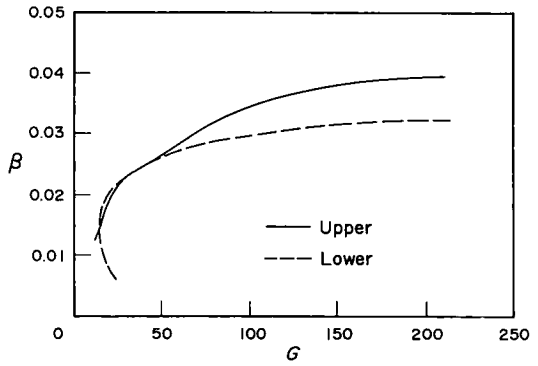

FIG. 19. Computed neutral stability curves in the (G, β) plane for the upper- and lower-branch solutions at $R = 0.34$.

implications of our numerical results, since a path of constant physical frequency corresponds to a path on the stability plane as a disturbance is convected downstream. The basic premise here is that the physical frequency of a disturbance will not change while the disturbance is still small; that is, in the valid range of linear stability theory.

When we consider the neutral stability curves in the (G, β) plane (or (G, B) plane) for two solutions corresponding to the upper- and lower-branch (multiple steady-state) solutions at the same value of R in the range $0.30 \leqslant R \leqslant 0.34$, we see that, in general, the neutral stability curve for the lower-branch solution intersects the curve for the upper-branch solution at three points $G_{\beta j}$, $j = 1, 2, 3$; see Table 3 and Figs. 15, 17, and 19. These intersection points are where each branch has the same neutral stability at one particular frequency. For $G < G_{\beta 1}$ or $G_{\beta 2} < G < G_{\beta 3}$ the first instability of the flow corresponding to a lower-branch solution occurs sooner than the first instability of the flow corresponding to an upper-branch solution; for $G_{\beta 1} < G < G_{\beta 2}$ or $G > G_{\beta 3}$ the reverse is true.

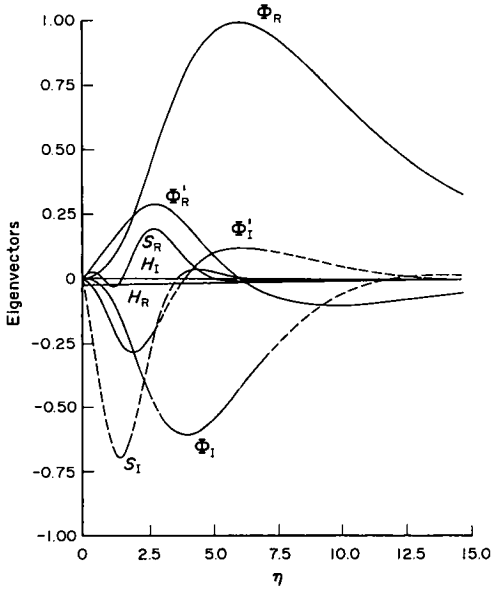

FIG. 20. Plots of eigenvector components vs η corresponding to the upper-branch solution at $R = 0.34$ for $\alpha = 0.1477$, $\beta = 0.014$, $G = 15.23$, and $\eta_\infty = 60$.

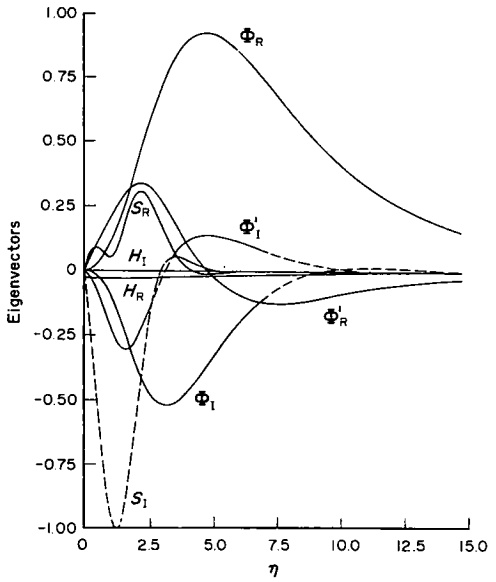

FIG. 21. Plots of eigenvector components vs η corresponding to the upper-branch solution at $R = 0.40$ for $\alpha = 0.1899$, $\beta = 0.0195$, $G = 19.62$, and $\eta_\infty = 40$.

It is interesting that, in general for various values of R, neutral stability for upper- compared to that for lower-branch solutions is more easily distinguished in the (G, α) plane (wave number vs Grashof number) than in the (G, β) plane (frequency vs Grashof number). In the (G, α) plane, at $R = 0.34$ the neutral stability curves for two upper- and lower-branch solutions intersect only at one point; see Fig. 18. However, for $R = 0.30$ and $R = 0.32$ the two stability curves corresponding to the upper- and lower-branch solutions in the (G, α) plane intersect each other at three points $G_{\alpha j}$, $j = 1, 2, 3$; see Table 2 and Figs. 14 and 16. The values of G at the points of intersection are not the same as those in the (G, β) plane.

The critical Grashof number for the lower-branch solution is much less than that for the corresponding upper-branch solution. This implies that the lower-branch solutions are less stable. Indeed the lower-branch solutions may not be observable. Nevertheless, the flow for some lower-branch solutions might be more stable at the initial stage of instability. For *some* disturbances, for example, those which are in a band of frequencies $B_1 < B < B_2$ with wave numbers $A_1 < A < A_2$ in the first crossing region (i.e. for both $G_{\beta 1} < G < G_{\beta 2}$ and $G_{\alpha 1} < G < G_{\alpha 2}$), the flow for the lower-branch solutions appears to be more stable than the flow for the corresponding upper-branch solutions. Thus, our results give an idea under what conditions the multiple steady-state solutions found in El-Henawy *et al.* [4] can exist and may be observable. The experimental data from Wilson and Vyas [11] for $R = 0.317$ and from Carey and Gebhart [12]

for $R = 0.254$ support the conclusion that oscillation between steady-state flows may exist, i.e. there may be oscillations between the upper- and lower-branch solutions. However, their experimental data only crudely fit these two solutions (see Figs. 8 and 9 in Carey and Gebhart [12] and Figs. 4–7 in Wilson and Vyas [11]).

As the density extremum parameter increases, the range of the second crossing region of G in the (G, β) plane (i.e. $G_{\beta 2} < G < G_{\beta 3}$) is significantly reduced from 49.85 at $R = 0.30$ to 11.52 at $R = 0.34$. Moreover, the corresponding range in the (G, α) plane (i.e. $G_{\alpha 2} < G < G_{\alpha 3}$) is also significantly reduced from 37.73 at $R = 0.30$ to 10.11 at $R = 0.32$. The second crossing region for the (G, α) plane no longer exists at $R = 0.34$ so that there is no common range of G corresponding to the second crossing region in both stability planes. As R approaches $R = 0.34$, the two neutral stability curves for the upper- and lower-branch solutions become distinct from each other: the shapes of their profiles differ and there are corresponding significant differences in their critical Grashof numbers G_{cr} and in their upper limits of wave number A_{max} (see Table 1). Thus, we conjecture that for the range $R > 0.34$, the neutral stability curves corresponding to the two solutions have only one point of intersection in the (G, α) and (G, β) planes and have no second crossing region in either the (G, α) and (G, β) planes. We also conjecture that the profiles of the curves become more distinctive and their G_{cr} values differ more significantly from each other as R increases from $R = 0.34$. We believe this is mainly because the G_{cr} and A_{max} values corresponding to the lower-branch solutions become extremely small and approach zero while the G_{cr} and A_{max} values corresponding to upper-branch solutions increase.

For a multiple steady-state problem, the initial condition is very important. Also, depending on the amplitude of the disturbance, the flow may jump from the lower-branch to the upper-branch solution of the base flow. However, the authors could not perform the stability analyses concerning the spatial or temporal amplifications (also, initial conditions). Thus, we could not understand these mechanisms. Our study is only confined to the neutral stability analysis.

For the range $0.29181 < R < 0.34$, one cannot easily judge from our results which flow is more stable under the action of *natural* disturbances (without experimentally introducing controlled disturbances). One flow is not more stable for a wide region of G, but only relatively more stable, at the stage of initial instability, for subregions of G than is the other flow. Thus, there may be oscillations between the upper- and lower-branch solutions for ranges of $R < 0.34$. There is a greater possibility, especially for R approaching 0.29181, to observe such oscillations. If $R \geqslant 0.34$, we believe oscillatory flows cannot exist and we conjecture that there is no possibility to observe the lower-branch solutions of the base flows, because the features characterizing their neutral stability are quite distinctive from those belonging to upper-branch solutions.

Some of the main features of the effects of the inside buoyancy force reversals in the region $0.29181 \leqslant R < 0.5$ upon natural convection adjacent to a vertical isothermal surface in cold water can be readily recognized from the results of our linear stability calculations. An increase in the magnitude of the inside buoyancy force reversals always causes the critical Grashof number to decrease significantly. It is easy to show that there is a destabilizing effect due to the characteristics of the buoyancy force. This effect is a consequence of the dependence of the number of points of inflection and their location, in the profile of velocity of the base flow, upon buoyancy force reversals.

If we exclude lower-branch solutions, we can show that the buoyancy force at $\eta = 0$ controls the curvature of the velocity profile by applying boundary conditions at $\eta = 0$ to the equation (4a):

$$f_b'''(0) = -\delta(|1-R|^q - |R|^q) \tag{20}$$

where $\delta = -1$ for downflow. The quantity $|1-R|^q - |R|^q$ represents the buoyancy force at the vertical surface.

From equation (20), we see that $f_b'''(0)$ is always positive for a flow whose velocity profile has two points of inflection, in the region $0.29181 \leqslant R < 0.5$. $f_b'''(0) = -1$ for a normal natural convection flow (i.e. $R = 0$, $q = 1$ and $\delta = +1$ for the Boussinesq situation), whose velocity profile has only one point of inflection. Let us call the first point of inflection $\eta_{P.I.1}$ and the second point of inflection $\eta_{P.I.2}$. If $\eta < \eta_{P.I.1}$, then $f_b'''(\eta) > 0$; if $\eta_{P.I.1} \leqslant \eta \leqslant \eta_{P.I.2}$, then $f_b'''(\eta) \leqslant 0$ and if $\eta > \eta_{P.I.2}$, then $f_b'''(\eta) > 0$. If $f_b'''(0) \to 0^+$, the corresponding $\eta_{P.I.1}$ and $\eta_{P.I.2} \to 0^+$. If $f_b'''(0) \leqslant 0$ for $R \geqslant 0.50$, only a single point of inflection exists. Thus, for an upper-branch solution, the buoyancy force at $\eta = 0$ controls the curvature of its velocity profile near $\eta = 0$.

There is only one point of inflection in the velocity profile of the base flow for $R = 0.50$, where the buoyancy force is unidirectionally downward. However, in the case of the flow region $0.29181 \leqslant R < 0.50$, two points of inflection always exist and these points shift toward $\eta = 0$ as the upward inside buoyancy force reversal becomes weaker. Accordingly, the heat transfer rate $-\theta_b'(0)$ increases as R decreases from 0.5 to 0.29181 (lower-branch solutions) and further increases as R increases from 0.29181 (upper-branch solutions). At the same time the critical Grashof number consistently increases.

REFERENCES

1. B. Gebhart, Buoyancy induced motions characteristic of applications in technology, *Trans. ASME, J. Fluid Engng* **101**, 5–28 (1979).
2. B. Gebhart, Y. Jaluria, R. L. Mahajan and B. Sammakia,

Buoyancy-induced Flows and Transport. Hemisphere, New York (1988).
3. U. Ascher, J. Christiansen and R. D. Russell, COLSYS—a collection code for boundary-value problems. In *Codes for Boundary-value Problems in Ordinary Differential Equations* (Edited by G. Goos and J. Hartmanis), Lecture Notes in Computer Science, Vol. 76, pp. 164–185. Springer, New York (1978).
4. I. El-Henawy, B. Gebhart, B. Hassard, N. Kazarinoff and J. Mollendorf, Numerically computed multiple steady states of vertical buoyancy-induced flows in cold pure water, *J. Fluid Mech.* **122,** 235–250 (1982).
5. P. R. Nachtsheim, Stability of free-convection boundary layer flows, NASA TN D-2089 (1963).
6. C. A. Hieber and B. Gebhart, Stability of vertical natural convection boundary layers: some numerical solutions, *J. Fluid Mech.* **48,** 625–646 (1971).
7. Y. Jaluria and B. Gebhart, On transition mechanisms in vertical natural convection flow, *J. Fluid Mech.* **66,** 309–337 (1974).
8. J. Y. Jang, Part II: The stability of a vertical natural convection boundary layer with temperature dependent viscosity. Doctoral dissertation, SUNYAB, Buffalo, New York (1983).
9. B. Gebhart and R. L. Mahajan, Instability and transition in buoyancy induced flows, *Adv. Appl. Mech.* **22,** 231–315 (1982).
10. B. Gebhart and J. C. Mollendorf, Buoyancy-induced flows in water under conditions in which density extremes may arise, *J. Fluid Mech.* **89,** 673–707 (1978).
11. N. W. Wilson and B. D. Vyas, Velocity profiles near a vertical ice surface melting into fresh water, *Trans. ASME, J. Heat Transfer* **10,** 313–317 (1979).
12. V. P. Carey and B. Gebhart, Visualization of the flow adjacent to a vertical ice surface melting in cold pure water, *J. Fluid Mech.* **107,** 37–55 (1981).
13. V. P. Carey, B. Gebhart and J. C. Mollendorf, Buoyancy force reversals in vertical natural convection flows in water, *J. Fluid Mech.* **97,** 279–297 (1980).
14. Z. H. Qureshi, Stability and measurements of fluid and thermal transport in vertical buoyancy induced flows in cold water. Doctoral dissertation, SUNYAB, Buffalo, New York (1980).
15. J. M. Higgins, Stability of buoyancy induced flow of water near the density extremum, adjacent to a vertical, isothermal surface. Doctoral dissertation, SUNYAB, Buffalo, New York (1981).
16. J. M. Higgins and B. Gebhart, The stability of vertical buoyancy induced flow in cold water, *Trans. ASME, J. Heat Transfer* **105,** 767–773 (1983).
17. Z. H. Qureshi and B. Gebhart, The stability of vertical thermal buoyancy induced flows in cold pure and saline water, *Int. J. Heat Mass Transfer* **29,** 1383–1392 (1986).
18. B. Gebhart and J. C. Mollendorf, A new density relation for pure and saline water, *Deep Sea Res.* **24,** 831–848 (1977).
19. J. M. Higgins and B. Gebhart, Measurements of instability and disturbance growth in vertical buoyancy induced flows in cold water, *Int. J. Heat Mass Transfer* **25,** 1397–1409 (1982).
20. Z. H. Qureshi and B. Gebhart, Measurements of fluid and thermal transport in vertical buoyancy induced flows in cold water, *Int. J. Heat Mass Transfer* **24,** 1503–1511 (1981).
21. I. M. El-Henawy, B. D. Hassard and N. D. Kazarinoff, A stability analysis of non-time-periodic perturbations of buoyancy induced flows in pure water near 4 C, *J. Fluid Mech.* **163,** 1–20 (1986).
22. P. Deuflhard and G. Bader, Multiple shooting techniques revisited, Preprint No. 163, Institut für Angewante Math., University of Heidelberg (1982).
23. H. Schlichting, *Boundary Layer Theory*, 7th Edn. McGraw-Hill, New York (1977).